Electrostatic and Association Phenomena in Aggregates of Polymers and Micelles

Gina A. Sorci and Wayne F. Reed*

Physics Department, Tulane University, New Orleans, Louisiana 70118

Received June 25, 2001. In Final Form: October 17, 2001

An automatic, continuous-mixing technique is introduced to measure light scattering and viscosity simultaneously over a wide range of solute concentrations in multicomponent systems. Behavior along arbitrary curves in component coordinates can be monitored. This technique is used to investigate the association and electrostatically based excluded-volume interactions that arise in solutions of interacting neutral polymers and charged micelles. In this study, the ionic surfactant sodium dodecyl sulfate (SDS) and a neutral polymer poly(vinylpyrrolidone) (PVP) were chosen. The SDS confers pseudopolyelectrolyte properties on the polymer/micelle aggregates (PSA), such as electrostatically enhanced second and third virial coefficients A_2 and A_3, respectively. The presence of a large A_3 is directly observed as a well-defined maximum in scattering intensity versus [PVP] under saturating SDS conditions. The electrostatically enhanced three-body effects represented by A_3 in light scattering are nearly 3 orders of magnitude greater than the corresponding three-body terms in viscosity. A viscosity effect reminiscent of the electroviscous effect seen for linear polyelectrolytes is observed, but it occurs under very different PSA concentration and solution ionic strength conditions.

Introduction

The goal of the current work is twofold: (1) to introduce an automatic dilution technique that allows continuous monitoring of changes in equilibrium behavior along arbitrary paths in component space and (2) to monitor the viscosity and light-scattering behavior of interacting polymers and micelles simultaneously and discern the different effects that association and electrostatics have. The effects of the electrostatically enhanced excluded volume should be quite different for light scattering, which depends on the values of the second and third virial coefficients A_2 and A_3, respectively, and for viscosity, in which equivalent radii and interparticle hydrodynamic interactions may be considerably smaller than those defining the virial coefficients.

The interactions of polymers and surfactants have been the subject of fundamental and applied research for many years. Studies have included both neutral and charged polymers and surfactants. Areas of growing interest include the interaction of oppositely charged linear and cross-linked polyelectrolytes and micelles[1−3] and hydrophobically modified polymers with micelles.[4,5] In many studies, varying degrees of cooperative and stoichiometric binding have been reported. Because of the complexity of polymer/colloid interactions, many different experimental techniques have been used, including light, neutron, and X-ray scattering, neutron reflectivity, EMF measurements, and microcalorimetry.[6,7]

There appears to be a general consensus that there is a critical aggregation concentration (CAC) of surfactant at which micelles begin to form a "bead necklace" on the polymer; there are, however, varied opinions about whether interactions occur below the CAC. There is also consensus that there is a polymer saturation point (PSP) beyond which no more added surfactant binds to the polymer. It is also generally agreed that the size of the micelles bound to the polymers is usually smaller than the size of the micelles in the free state.[8,9]

Gel permeation chromatography (GPC) has been used to analyze polymer/surfactant properties, especially surfactant/polymer binding ratios. Rodenhiser and Kwak used GPC to determine surfactant binding coefficients[10] via the vacant peak in sodium dodecyl sulfate (SDS) when poly(ethylene oxide) (PEO) was injected into an aqueous eluent containing SDS. Ionic strengths and Donnan equilibrium effects have also been studied using GPC.[11,12] Pisarcik et al. found that aggregates composed of sodium hyaluronate and nonionic surfactants reached maximum mass at the surfactant CMC, but the mass decreased as surfactant concentration increased further. For ionic surfactants, the mass increased and then reached a plateau.[13]

Purcell et al.[14] used neutron reflectivity in an index-nulled aqueous solvent to determine that there was both a strong interaction of SDS and poly(vinylpyrrolidone) (PVP) at the surface and that there were interactions between surfactants and polymers even below the CAC. The latter conclusion was also reached by Minatti et al. using light scattering.[15] It has also been shown by

* Corresponding author.

(1) Isogai, N.; Narita, T.; Chen, L.; Hirata, M.; Gong, J. P.; Osada, Y. *Colloids Surf.* **1999**, *147*, 189.
(2) Yoshida, K.; Dubin, P. L. *Colloids Surf.* **1999**, *147*, 161.
(3) Pisarcik, M.; Toyoko, I.; Devinsky, F.; Lacko, I. *Colloids Surf.* **2001**, *183*, 555.
(4) Panmai, S.; Prud'homme, R. K.; Peiffer, D. G., *Colloids Surf.* **1999**, *147*, 3.
(5) Bloor, D. M.; Qan-Yunus, W. M. Z.; Wan-Badhi, W. A.; Li, Y.; Holzwarth, J. F.; Wyn-Jones, E. *Langmuir* **1995**, *11*, 3395.
(6) *Interactions of Surfactants with Polymers and Proteins*; Goddard, E. D., Ananthapadamanabhan, K. P., Eds.; CRC Press: Boca Raton, FL, 1993.
(7) *Colloid−Polymer Interactions*; Farinato, R. S., Dubin, P. L., Eds.; Wiley & Sons: New York, 1999.
(8) Cabane, B.; Duplessix, R. *J. Phys.* **1982**, *43*, 1529.
(9) Lianos, P.; Lang, J.; Strazielle, C.; Zana, R. *J. Phys. Chem.* **1982**, *86*, 1019.
(10) Rodenhiser, A. P.; Kwak J. C. T. *Colloids Surf.* **1999**, *150*, 191.
(11) Veggeland, K.; Austad, T. *Colloids Surf.* **1993**, *76*, 73.
(12) Veggeland, K.; Nilsson, S. *Langmuir* **1995**, *11*, 1885.
(13) Pisarcik, M.; Imae, T.; Devinsky, F.; Lacko, I. *Colloids Surf.* **2001**, *183*, 555.
(14) Purcell, I. P.; Lu, J. R.; Thomas, R. K.; Howe, A. M.; Penfold, J. *Langmuir* **1998**, *14*, 1637.
(15) Minatti, E.; Norwood, D. P.; Reed, W. F. *Macromolecules* **1998**, *31*, 2966.

10.1021/la0109718 CCC: $22.00
Published on Web 12/22/2001

isothermal titration calorimetry that certain nonionic surfactants can remove bound SDS from PVP and in the process form mixed micelles both on the polymer and in the bulk.[16] This result has been used as further evidence that the attraction between SDS and PVP is chiefly electrostatic in character because mixed micelles with smaller charges associate less strongly with PVP.

Recent work in our group focused on the binding properties of micelles to neutral polymers[17] and the electrostatic behavior of the aggregates themselves.[15] It was concluded that the micelles bind to the polymer in rather deep, localized energy wells and that there is a surprising lack of anticooperativity.

The adaptation of automatic, continuous dilution to the study of equilibrium properties of polymer/micelle interactions grew out of our ongoing program involving realtime studies of nonequilibrium processes, such as polymerization reactions,[18,19] degradation,[20−22] and dissolution.[23] We used the technique for equilibrium characterization initially as a means of automating Zimm plotting and viscosity determinations for polymers.[24] Later, we used the technique to observe how polyelectrolyte conformations and interactions are affected by the solution ionic strength.[25]

In this work, attention is focused on the interaction of a neutral polymer, PVP, with an anionic surfactant, SDS. Considerable work has been done on different aspects of this particular system, including surface adsorption studied by neutron reflection,[14] phase behavior,[12] and other methods.[16,26,27] Multicomponent systems often manifest complex phase behavior, and the determination of the phase diagram is usually a tedious process. The automatic, continuous-mixing technique allows parametrized paths in the component space to be explored. The current system contains up to four components—water, a simple electrolyte, a surfactant, and a neutral linear polymer—with several phases in equilibrium. The surfactant can exist in molecular form, in micelles, and in association with the polymer. There is good evidence that surfactants can bind to polymers individually or as complete micelles. Structures that involve surfactants bound in any way to polymers will be denoted polymer/surfactant aggregates (PSA) In this work, selected paths in component space are explored to determine binding, electrostatic, and interaction properties of the PSA, with emphasis on how these affect A_2, A_3, and viscosity.

Materials and Methods

Automatic Mixing Technique. The use of a programmable mixing pump ensures that any parametrized path can be explored for solutions composed of a simple salt, a surfactant, and a polymer. While this technique offers a rich variety of approaches, we limit ourselves in this work to three paths:

(i) Increasing PVP concentration with constant surfactant and salt concentrations. This path allows us to explore the region beyond the PSP and then to fall below the saturation limit.

(ii) Increasing SDS concentration with constant polymer and salt concentrations. This path allows us to start with pure polymer, which is then gradually charged by SDS monomers. Beyond the CAC, the polymer should begin to aggregate with the micelles. At high enough SDS concentration, the PSP should be crossed and the PVP will be fully saturated.

(iii) Increasing the salt content while keeping the surfactant concentration fixed and the PVP concentration low. Following these paths, it will be possible to extrapolate to [PVP] = 0, yielding both the fractional composition of the PSA in terms of PVP and SDS and A_2 as a function of ionic strength. Hence, the electrostatic aspects can be directly queried with these paths.

The experimental setup consisted of an ISCO 2360 gradient mixer coupled with an ISCO 2350 isocratic pump. The mixer allows programmable mixing of liquids from up to three reservoirs, permitting many types of dilutions. The water was taken from a Modulab analytical research UF/polishing system with a 0.1 μm outlet filter and a conductivity of less than 0.055 μmho/cm and was prefiltered with a 0.22 μm Millipore filter just before the solutions were made. A 10 μm filter was placed in the reservoir with the solvent (i.e., pure water, water with salt, water with SDS, etc.). Both the solvents and polymer solutions were then prepared with the filtered water. After the pump, there was an inline 0.5 μm frit filter in a 0.5 in. diameter housing This pump was followed by a Wyatt Dawn DSP F photometer used in flow mode, a single-capillary viscometer (built in-house), and Waters 410 refractometer. For some experiments, a light-scattering flow cell (built in-house), previously used for online monitoring of polymerization reactions, was also connected in series. Addition of a 1 in. diameter stainless steel filter housing fitted with a 0.45 μm Millipore Corporation membrane filter significantly improved data quality, even at low scattering angles. The data were collected and analyzed using custom software.

The mixing characteristics and time constant of the apparatus are of critical importance for ensuring accurate, reproducible results. These were assessed by connecting an HPLC-type injector with a 10 μL loop both before and after the pumps. In the latter case, the injector was also connected to the loop before and after the filters, and both solutions containing 100 mM NaCl and 0.002 g/cm^3 PVP were injected. The profiles were invariably a convolution of a Gaussian (due to lateral diffusion in the flow path) and an exponential profile (due to mixing-chamber behavior). A flow rate of 1 mL/min was used throughout. The mixing volume was approximately 2.75 mL. After this analysis, a linear gradient lasting 120 min was established for programming the mixing pump; the gradient covered the range from pure solvent to the concentration of polymer in the second reservoir (and salt and/or SDS when appropriate). The reproducibility and independence of results on gradient period and flow rate were verified by ramping the polymer concentration from pure solvent to polymer-reservoir concentration to pure solvent) and confirming that the data overlapped. If the gradients were made too quickly, the results did not overlap.

Before performing experiments, detectors were purged with the solvent to be used. At the beginning of each experiment, after stabilizing the detectors with pure solvent, data was collected so as to have a baseline for each instrument before the gradient began.

Gel Permeation Chromatography (GPC). GPC was performed on a system with Shodex SB804-HQ and SB806-HQ columns in series and three detectors. The differential refractometer was an Erma ERC 7522. The viscometer was a single-capillary device built in-house and previously described in detail.[28] The multiangle light-scattering photometer was also built in-house and has been used previously in batch-flow mode for online monitoring of polymerization reactions[18,19] automatic equilibrium characterization of polymers,[24] and the effect of changing ionic strength on polyelectrolyte conformations, interactions, and hydrodynamics.[25] The instrument was adapted to GPC for the

(16) Li, T.; Xu, R.; Bloor, D. M.; Penfold, J.; Holzwarth, J. F.; Wyn-Jones, E. *Langmuir* **2000**, *16*, 8677.
(17) Norwood, D. P.; Minatti, E.; Reed, W. F. *Macromolecules* **1998**, *31*, 2957.
(18) Florenzano, F. H.; Strelitzki, R.; Reed, W. F. *Macromolecules* **1998**, *31*, 7226.
(19) Giz, A.; Giz, H.; Brousseau, J. L.; Alb, A.; Reed, W. F. *Macromolecules* **2001**, *34*, 1180.
(20) Reed, C. E.; Reed, W. F. *J. Chem. Phys.* **1989**, *91*, 7193.
(21) Ghosh, S.; Reed, W. F. *Biopolymers* **1995**, *5*, 435.
(22) Ganter, J. L.; Reed, W. F. *Biopolymers* **2001**, *59*, 226.
(23) Michel, R. C.; Reed, W. F. *Biopolymers* **2000**, *53*, 19.
(24) Strelitzki, R.; Reed, W. F. *J. Appl. Polym. Sci.* **1999**, *73*, 2359.
(25) Bayly, E.; Brousseau, J. L.; Reed, W. F. *Int. J. Polym. Anal. Charact.*, in press.
(26) Bianca, S.; D'Aprano, A.; Segre, A. L.; Proietti, N. *Langmuir* **1997**, *13*, 6612.
(27) Zanette, D.; Ruzza, A. A.; Froehner, S. J.; Minatti, E. *Colloids Surf.* **1996**, *106*, 100.
(28) Norwood, D. P.; Reed, W. F. *Int. J. Polym. Anal. Charact.* **1997**, *4*, 99.

Table 1. Properties of PVP As Determined by GPC

designation	M_w (kg/mol)	M_w/M_n	M_z/M_w	$[\eta]$ cm^3/g
50 KDa	55	4.6	4.4	38
1 MDa	1000	3	2.1	142
2 MDa	1850	2.1	1.8	207

first time in this work. Its performance was checked against a Polymer Laboratory PEO standard with a molecular weight 51 kg/mol.

Compounds. Electropure-grade SDS was purchased from Polysciences. PVP was purchased from Sigma Aldrich and International Specialty Products (K-120 and K-30). Table 1 gives a summary of the GPC analysis of each PVP used. The differential refractive index ($\partial n/\partial c$) was 0.173 and 0.122 for PVP and SDS, respectively.

Analysis of Light Scattering and Viscosity in Multicomponent Systems. The scattering and viscosity measured in this work involve complex multicomponent systems. The species in equilibrium include PVP polymer chains, SDS monomers and micelles, and PSA. In ref 17, an extensive study of multicomponent scattering from these systems was made. The total excess scattering (i.e., total scattering − pure-solvent scattering) from a multicomponent system is given by the proportionality[29]

$$I(q) \propto \sum_{i,j=1}^{s} \frac{\partial n}{\partial c_i} S_{ij}(q) \frac{\partial n}{\partial c_j} \tag{1}$$

where s is the number of components in the system, $\partial n/\partial c_i$ is the differential refractive index (or optical contrast) of species i and c_i and c_j are the concentrations in g/cm^3 of species i and j, respectively. S_{ij} represents the partial structure factors given in matrix form by[30]

$$S_{ij} = \delta_{ij} + (N_i N_j)^{1/2} \int [g(\vec{r}_{ij}) - 1]\, e^{i\vec{q}\cdot\vec{r}_{ij}} d^3 r_{ij} \tag{2}$$

where N_i and N_j are the particle densities of species i and j, respectively, δ_{ij} is the Kronecker delta function, and $g(r_{ij})$ is the interparticle correlation function given by

$$g(r_{ij}) = \exp[-U(r_{ij})/k_B T] \tag{3}$$

where $U(r_{ij})$ is the potential of mean force between particles i and j separated by a center-to-center distance r_{ij}. For repulsive interactions $S_{ij} < 0$ for $i \neq j$, meaning that the cross-term decreases scattered intensity, as do positive virial coefficients in homogeneous systems. In solutions composed of SDS monomers and micelles, simple salts, polymers, and polymer/micelle aggregates, the only significant scatterers are the micelles, polymers, and PSA. Furthermore, because all the polymers are the same species, albeit polydisperse, they exist as PSA whenever micelles are present; therefore, the total excess scattering is

$$I_{total} = S_{aa}(q)\, P_a(q)\, K_a c_a M_a + 2S_{am}(q)\, [P_a(q)\, K_a c_a M_a\, P_m(q)\, K_m c_m M_m]^{1/2} + S_{mm}(q)\, P_m(q)\, K_m c_m M_m \tag{4}$$

where the a and m subscripts refer to PSA and micelles, respectively, and the $P(q)$s are the scattering form factors of the particles. Our main goal in this work is to determine properties of the PSA. Hence, the micellar term and the cross-term must be subtracted. It is straightforward to measure the micelle term using solutions containing only SDS. The cross-term measurement poses more of a problem, and short of in-depth contrast studies using different polymers and solvents, it is easier to estimate when it may be important. It was proven in ref 17 that the cross-term is usually negligible.

The lowest-order approximation to $S(q)$ can be written in terms of the q-independent second virial coefficient A_2 as

$$S_{ij} \approx (\delta_{ij} + 2A_{2,ij}\sqrt{M_i c_i M_j c_j})^{-1} \tag{5}$$

so that the ratio of the absolute value of the cross-term to the PSA scattering term is

$$\left|\frac{\text{cross-term}}{\text{PSA-term}}\right| \cong \frac{1 + 2A_{2,aa}c_a M_a}{A_{2,am}c_a M_a}\left(\frac{P_m(q)K_m}{P_a(q)K_a}\right)^{1/2} < 1 \tag{6}$$

where the term in parentheses is on the order of unity. Hence, the ratio of terms (eq 6) depends on the ratio of $A_{2,aa}$ (from the PSA/PSA interaction) to $A_{2,am}$ (from the PVP/SDS interaction). A_2 is often expressed as

$$A_{2,ij} = \frac{N_A \beta_{ij}}{2M_i M_j} \tag{7}$$

where β_{ij} is the binary cluster integral on the right side of eq 2. β_{ij} is also the excluded volume between two spheres and is equivalent to interactions between particles i and j. As an estimated lower limit, $\beta_{ij} \propto (\langle S^2\rangle^{1/2} + r_m)^3$, in which $\langle S^2\rangle^{1/2}$ is the root-mean-square radius of gyration of the polymer and r_m is the micelle radius . With large PVP polymers, $R_g \approx 1$ nm and $r_m \approx 50$ nm. Because $M_a \approx 200\, M_m$, the net effect is that $A_{2,a,m}$ will be more than an order of magnitude greater than $A_{2,a,a}$. Hence, $S_{am} \approx 0.1$ and will become significant only when $2A_{2,a,a}c_a M_a \ll 1$ (i.e., at very low c_a, or for small values of $A_{2,aa}$ and M_a). The upper limit is a volume computed on the basis of the electrostatically enhanced radii of the polymer and the micelle, in which case $A_{2,am}$ will be about 2 orders of magnitude smaller than $A_{2,aa}$. It is beyond the scope of this work to explore the cross-terms in depth, but the continuous-dilution technique presented here should make such studies experimentally viable and efficient.

When the cross-term is negligible, the scattering from the PSA can be closely approximated by subtracting micelle and solvent scattering from the total scattering. After the scattering due to the PSA has been computed, it is convenient to work within the well-known Zimm approximation,[31] which expresses total excess scattering $I(q,c)$ in terms of the scatterer's mass M, concentration c_p (g/cm^3), and second and third virial coefficients A_2 and A_3, respectively:

$$\frac{Kc_p}{I(q,c_p)} = \frac{1}{MP(q)} + 2A_2 c_p + [3A_3 Q(q) - 4A_2^2 MP(q)(1 - P(q))]c_p^2 \tag{8}$$

where $Q(q)$ involves a sum of complicated Fourier transforms of the segment interactions that define A_3. This equation forms the basis of the well-known Zimm plot, which at low values of c_p and for $q^2\langle S^2\rangle_z \ll 1$ can be written for a polydisperse polymer population as

$$\frac{Kc_p}{I(q,c_p)} = \frac{1}{M_w}\left(1 + \frac{q^2\langle S^2\rangle_z}{3}\right) + 2A_2 c_p + O(c_p^2) \tag{9}$$

which permits direct determination of M_w, A_2, and the z-averaged mean square radius of gyration $\langle S^2\rangle_z = R_g$. K is an optical constant given for vertically polarized incident light by

$$K = \frac{4\pi^2 n^2 (\partial n/\partial c_p)^2}{N_A \lambda^4} \tag{10}$$

where n is the solvent index of refraction, λ is the wavelength of the incident light in vacuo, and q is the usual scattering-wave vector ($q = (4\pi n/\lambda)\sin(\theta/2)$, θ = the scattering angle).

In the limit $q = 0$, A_3 can be found via

(29) Benmouna, M.; Vilgis, T.; Hakem, F.; Negadi, A. *Macromolecules* **1991**, *24*, 6418.

(30) Higgins, J. S.; Benoit, H. C. *Polymers and Neutron Scattering*; Clarendon Press: Oxford, U.K., 1994; pp 119−120.

(31) Zimm, B. H. *J. Chem. Phys.* **1948**, *16*, 1093.

$$\frac{Kc_p}{I(q,c_p)} = \frac{1}{M_w} + 2A_2c_p + 3A_3{c_p}^2 \tag{11}$$

In analyzing the data for PSA, the concentration of PSA, c_{PSA}, is needed for substitution in eq 5. c_{PSA} is given by

$$c_{PSA} = c_p(1 + r) \tag{12}$$

r is the ratio of surfactant mass to polymer mass in PSA:

$$r \equiv \left.\frac{M_{SDS}}{M_p}\right|_{\text{in PSA}} = \left.\frac{c_{SDS}}{c_p}\right|_{\text{in PSA}} \tag{13}$$

r is one of the most important parameters of the PSA. Because c_p and K are known for the polymer, it is convenient to find the relationship between the easily computed $Kc_p/I(q,c_p)$ and r, and between the other particle parameters and r.

The Clausius−Mossotti equation is

$${n}^2 - {n_0}^2 = 4\pi\alpha \tag{14}$$

where α is the polarizability of the PSA and n_0 is the pure-solvent index of refraction. The first-order expansion is

$$n = n_0 + \Delta n = n_0 + \sum_i \frac{\partial n}{\partial c_i} c_i \tag{15}$$

where the summation is over the total number of components in the composite scatterer. In the noninteracting limit, the excess scattering is proportional to α^2, that is

$$I(q) \propto \left(\sum_i \frac{\partial n}{\partial c_i} c_i\right)^2 \tag{16}$$

which allows the optical constant for the two-component K_{PSA} to be expressed as

$$K_{PSA} = \frac{4\pi^2{n_0}^2(\partial n/\partial c_p)^2(1 + \delta r)^2}{N_A\lambda^4(1 + r)^2} = K\frac{(1 + \delta r)^2}{(1 + r)^2} \tag{17}$$

where K is the value obtained by using $\partial n/\partial c_p$ of the polymer in the definition of K and

$$\delta \equiv \frac{\left(\frac{\partial n}{\partial c_{SDS}}\right)}{\left(\frac{\partial n}{\partial c_p}\right)} \tag{18}$$

This relationship can be shown to be formally equivalent to the expressions obtained for light scattering from copolymers by Stockmayer and others.[32,33] From the point of view of scattering, the problem of the surfactant and the polymer associating into an aggregate is similar to that of two comonomer species with different values of $\partial n/\partial c$. The advantage in the PSA case is that the mass of the polymer is easily found, whereas for a copolymer, experiments must usually be done in three different solvents to find the weight fractions of the comonomers and the M_w of the copolymer.

The scattering due to only the PSA is

$$\frac{Kc_p}{I_{PSA}(q,c_p)} = \frac{1}{(1 + \delta r)^2}\left\{\frac{1}{M_{w,p}}\left(1 + \frac{q^2\langle S^2\rangle_z}{3}\right) + 2A_2c_p(1 + r)^2 + 3A_3{c_p}^2(1 + r)^3\right\} \tag{19}$$

where the relation

$$M_{w,PSA} = M_{w,p}(1 + r) \tag{20}$$

has been used. A_2 and A_3 refer to the interactions between PSA.

Because $M_{w,p}$ is known, r can be determined directly from the $Kc_p/I_{PSA}(q,0)$ intercept. Similarly, once r has been found, A_2 can be computed:

$$A_2 = 0.5\frac{(1 + \delta r)^2}{(1 + r)^2}\frac{\partial\left[\frac{Kc_p}{I_{PSA}}\right]}{\partial c_p} \tag{21}$$

The computation of $\langle S^2\rangle_z$ is independent of r and is given simply by

$$\langle S^2\rangle_z = 3\frac{\frac{\partial\left[\frac{Kc_p}{I_{PSA}(q,0)}\right]}{\partial q^2}}{\left[\frac{Kc_p}{I_{PSA}(0,0)}\right]} \tag{22}$$

Concerning viscosity-data analysis, the assumption is made that the PSA contribution to the viscosity is large and the SDS contribution is negligible. This assumption is experimentally justified. The total solution viscosity due to the concentration of PSA and the intrinsic viscosity of PSA, $[\eta]_{PSA}$, is given by

$$\eta = \eta_s[1 + [\eta]_{PSA}c_{PSA} + \kappa_{H1}{[\eta]_{PSA}}^2{c_{PSA}}^2 + \kappa_{H2}{[\eta]_{PSA}}^3{c_{PSA}}^3 + O({c_{PSA}}^4)] \tag{23}$$

where η_s is the pure-solvent viscosity and κ_{H1} and κ_{H2} are constants related to the two- and three-body hydrodynamic interactions between polymer chains, respectively. κ_{H1} is typically about 0.4 for neutral coil polymers.[34] The intrinsic viscosity is the extrapolation of the reduced viscosity of PSA, $\eta_{r,PSA}$, to zero concentration and zero shear rate. $\eta_{r,PSA}$ can be computed, in principle, directly from the voltage of a single-capillary viscometer (a differential pressure transducer) at every point i, without the need of an instrumental calibration factor, in terms of the viscometer baseline voltage V_b (solvent viscosity including SDS and salt) and the concentration of PSA at point i, $c_{PSA,i}$:

$$\eta_{r,PSA,i} = \frac{V_i - V_b}{c_{PSA,i}V_b} \tag{24}$$

This computation is possible because the output of the viscometer is directly proportional to the pressure drop across the capillary of internal radius R and length L, which in turn is directly proportional to the total solution viscosity via Poisseuille's equation:

$$\eta = \frac{\pi R^4 P}{8LQ} \tag{25}$$

Q is the flow rate (cm^3/s) through the capillary. The average shear rate in the capillary is

$$\dot{\gamma}_{ave} = \frac{8Q}{3\pi R^3} \tag{26}$$

In the method presented here, it is possible to extrapolate $\eta_{r,PSA}$ to $c = 0$, although the average shear rate will remain finite at about 860 s^{-1} for $Q = 1$ mL/min and $R = 0.0254$ cm. Fortunately, shear effects diminish with diminishing c. It is standard practice in size exclusion chromatography(SEC) coupled to viscometric detectors to approximate $[\eta]$ from the values of η_r determined at finite, low c and finite shear rate. Where shear thinning may occur, the values of η_r and $[\eta]$ will represent lower bounds on these quantities.

(32) Stockmayer, W. H.; Moore, L. D.; Fixman, M.; Epstein, B. N. *Polym. Sci.* **1955**, *16*, 517.

(33) Bushuk, W.; Benoit, H. *Can. J. Chem.* **1958**, *36*, 1616.

(34) Huggins, M. L. *J. Am. Chem. Soc.* **1942**, *64*, 2716.

As in light scattering, the concentration of polymer is known. In eq 27, η_r is computed using c_p rather than c_{PSA} in the denominator of eq 24. Because these concentrations are related to each other by eq 12, η_r is related to $[\eta]_{PSA}$ by

$$\eta_r = [\eta]_{PSA}(1 + r) + \kappa_{H1}(1 + r)^2[\eta]_{PSA}^2 c_p + \kappa_{H2}(1 + r)^3[\eta]_{PSA}^3 c_p^2 + \ldots \quad (27)$$

The Flory−Fox relation for polymers in theta solvents can be used as a starting point to relate $[\eta]$ to polymer dimensions.

$$[\eta]_{PSA} = \frac{\Phi_\eta}{M_{PSA}}(\sqrt{6}R_g)^3 \quad (28)$$

where the root-mean-square radius of gyration is defined as R_g for short-hand purposes ($R_g = \langle S^2 \rangle^{1/2}$) and $\Phi_\eta = N_A/2.35 = 2.56 \times 10^{23}$ is the Flory−Fox parameter. In non-θ solvents, $[\eta]$ depends on R_g^3, but the prefactor in eq 28 increases as $N^{3(\nu-1)}$ to reflect excluded-volume effects. N is the number of monomers (or statistical segment lengths) in the polymer, and ν is the scaling exponent in

$$R_g = AM^\nu \quad (29)$$

$\nu = 0.5$ in θ solvents and about 0.6 in good solvents. Using the relationship between $M_{w,p}$ and $M_{w,PSA}$ and combining eq 27 with eq 28 for up to two-body interactions yields

$$\eta_r = \left(\frac{6.27N_A}{M_p}\right)R_g^3 + \kappa_{H1}\left(\frac{6.27N_A}{M_p}\right)^2 c_p R_g^6 \quad (30)$$

Hence, η_r depends only on R_g^3 of the PSA, which is directly proportional to the hydrodynamic volume and the hydrodynamic interaction factor κ_{H1}. Both of these parameters can be obtained from the viscosity data without explicit knowledge of r.

Results and Discussion

Raw Data Trends. It is instructive to first examine the raw scattering and viscosity data under varying PVP, SDS, and NaCl concentrations before attempting to analyze our results so that we may easily detect the observable trends.

Figure 1a shows scattering intensity versus c_p for a series of 1 MDa PVP solutions: in pure water with 0.0005 and 0.00025 g/cm^3 SDS, and in 100 mM NaCl with 0.01 g/cm^3 SDS. There are several striking features. First, a well-defined maximum occurs when SDS is present, compared to the case of pure PVP where only a very broad, shallow maximum is seen. Second, the scattering intensity of the aqueous SDS/PVP solution is up to 10 times lower than the scattering intensity of the aqueous PVP solution. When NaCl is present in the SDS/PVP solution, the scattering is far higher than that in all the other cases. Third, the scattering intensity in the SDS/PVP solutions occurs at smaller values of [PVP] than does that in aqueous PVP solutions. At 0.00025 g/cm^3 SDS, there is a secondary minimum at about 0.004 g/cm^3 of PVP.

The inset to Figure 1a shows data for 50 kDa PVP in pure water and in 0.01 g/cm^3 SDS solution with no added salt. A secondary minimum in the SDS solution occurs at a concentration about 4 times higher than that of the 1 MDa case.

Figure 1b shows the raw viscosity data for solutions from Figure 1a. When SDS is present with no salt, the viscosity increases significantly faster than for aqueous PVP solution or PVP/SDS/100 mM NaCl. All curves involving SDS have an inflection point, which is discussed below in terms of desaturation of the PSA.

The behavior in Figure 1a and b can be consistently interpreted from the point of view of electrostatic and

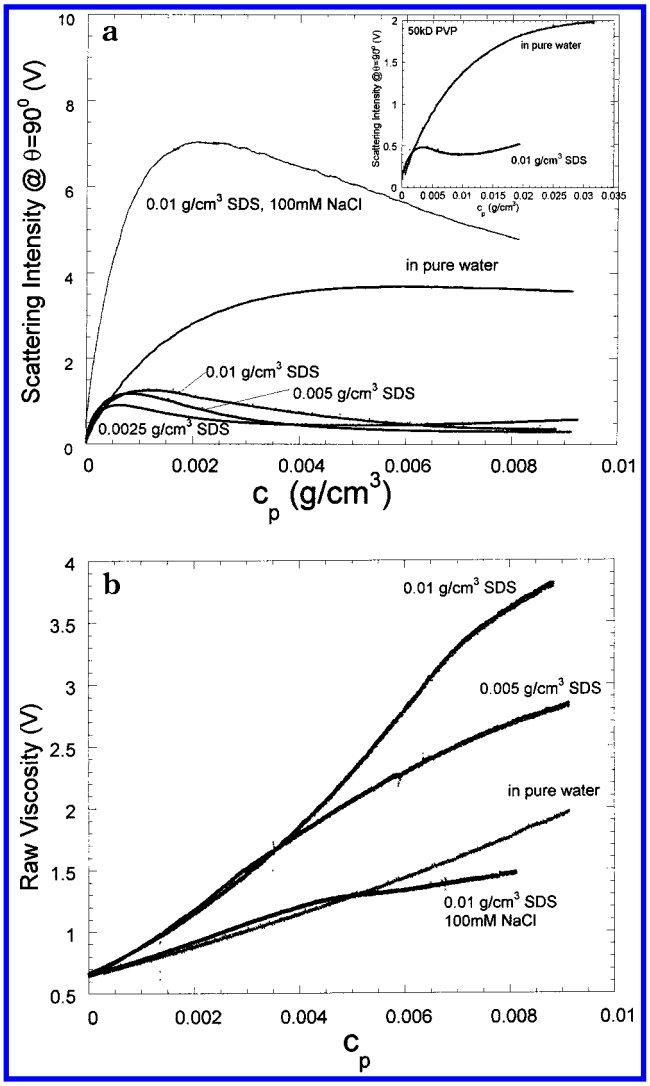

Figure 1. (a) Raw light-scattering data for 1 MDa PVP under a variety of solvent conditions. The inset shows raw scattering for 50 kDa PVP. (b) Raw viscosity data for experiments from Figure 1a.

association effects. The PVP at low concentration is saturated with SDS, which turns the otherwise neutral PVP into a quasi-polyanion that displays scattering and viscosity behavior qualitatively similar to that of a linear polyanion. The idea of a pseudopolyelectrolyte has been previously invoked[15,35] (the identification of the PSA for PVP/SDS as a polyanion was made in ref 17). Electrostatic effects cause an expansion of the polyanion coil, leading to increased values of $\langle S^2 \rangle_z$, A_2, A_3, and the hydrodynamic volume, as reflected in increased $[\eta]$ and total solution viscosity. The consistently lower scattering intensity with SDS in the absence of salt shows the effects of increased A_2 and A_3. The sharp maximum in the scattering is another vivid demonstration of the electrostatically enhanced A_3 compared to the neutral A_3. From the $q = 0$ limit of eq 11, A_3 is related to A_2 and M_w via the concentration of polymer at the scattering maximum, $c_{p,max}$, by

$$A_3 = \frac{1}{3(1 + r)^3 M_{w,PVP}\, c_{p,max}(q = 0)^2} \quad (31)$$

Equations 12 and 19 have been used to relate c_p to c_{PSA}

(35) Dubin, P. L.; Gruber, J. H.; Xia, J.; Zhang, H. *J. Colloid Interface Sci.* **1992**, *148*, 35.

Table 2. Association (*r*), Virial Coefficients, and Viscosity Characteristics of Pure PVP and PSA Composed of PVP/SDS

	r	A_2 (10^{-4} cm^{3}M/g^2)	$A_{3,\mathrm{fit}}$ (cm^{6}M/g^3)	ϵ	$A_{3,c_{p,max}}$ (cm^{6}M/g^3)	ϵ	η_r ($c_p = 0$) (cm^3/g)	$d\eta_r/dc_p$	κ_{H1}	$[\eta]$ (cm^3/g)
1 MDa, pure water		3.67 ± 1%	0.013 ± 8%	0.158 ± 8%	0.0128 ± 7%	0.153 ± 8%	169 ± 2%	7325 ± 10%	0.289 ± 11%	169
1 MDa, 1% SDS	0.414 ± 7%	13.5 ± 3%	0.298 ± 9%	0.265 ± 11%	0.171 ± 26%	0.152 ± 27%	365 ± 2%	58 367 ± 2%	0.438 ± 4%	258
1 MDa, 0.5% SDS	0.525 ± 6%	14.8 ± 6%	0.412 ± 13%	0.304 ± 17%	0.285 ± 8%	0.210 ± 15%	365 ± 1%	43 348 ± 2%	0.325 ± 2%	171
1 MDa, 1%SDS, 100 mM NaCl	1.55 ± 1%	1.85 ± 4%	0.0083 ± 4%	0.392 ± 4%	0.011 ± 7%	0.559 ± 10%	255 ± 2%	12 769 ± 5%	0.196 ± 2%	100
1 MDa, 0.25%SDS	0.634 ± 5%	11.6 ± 2%	0.446 ± 6%	0.536 ± 7%	0.556 ± 24%	0.669 ± 24%	360 ± 1%	18 214 ± 8%	0.143 ± 8%	220
50 kDa, pure water		9.91 ± 6%					37 ± 3%	551 ± 8%	.389 ± 9%	37
50 kDa, 1% SDS	0.398 ± 5%	36.3 ± 8%	0.292 ± 6%	0.709 ± 17%	0.265 ± 17%	0.636 ± 23%	46 ± 4%	1217 ± 7%	.575 ± 8%	34
2 MDa, pure water		3.41 ± 1%	0.019 ± 4%	0.159 ± 10%	0.0176 ± 28%	0.146 ± 29%	215 ± 2%	8193 ± 8%	0.177 ± 9%	215
2 MDa, 1% SDS	0.649 ± 5%	7.91 ± 9%	0.182 ± 10%	0.281 ± 20%	0.174 ± 15%	0.269 ± 24%	535 ± 1%	94 116 ± 3%	0.328 ± 4%	324

and $M_{w,PVP}$ to $M_{w,PSA}$. These A_3 values are shown in Table 2. The large scattering intensity when salt is added indicates the significantly greater mass of PSA compared to pure PVP.

In the inset to Figure 1a, the maximum in light scattering occurs at higher PVP concentration for lower M_w, which is consistent with eq 31 if A_3 is taken as approximately independent of M. An interesting feature of the 50 kDa PVP and the 1 MDa PVP in 0.00025 g/cm^3-SDS is that after the maximum is reached a minimum is reached at a higher c_p. This behavior is almost certainly due to desaturation of the PVP. Increasing c_p leads to a lower charge on the PVP/SDS aggregate, thus lowering A_2 and A_3 and allowing the total scattering intensity to rise.

Figure 2a shows the scattering intensity and η_r versus c_{SDS} for a 2 MDa PVP concentration of 0.002 g/cm^3 with no added salt. The striking feature is that as SDS is added the intensity decreases initially before reaching a minimum and gradually increasing. This behavior agrees with that reported previously[15] and is also consistent with the pseudopolyelectrolyte picture of the PSA. Namely, as SDS is added and associates with PVP, the PSA becomes electrically charged, leading to an increase in the electrostatic excluded volume (EEV). This increase in the EEV corresponds to increases in A_2 and A_3 such that the terms $2A_2c_p + O(c_p^2)$ increase more quickly than M_w increases; therefore, scattering is suppressed.

Another conclusion from Figure 2a is that SDS and PVP begin to associate as soon as any SDS is present. This behavior is suggested by the fact that the scattering intensity begins to fall as soon as SDS is added (i.e., well before the putative CAC). Other work that supports the notion of pre-CAC interaction may be found in refs 14, 15, and 17. Support for the notion of no pre-CAC interaction includes EMF measurements of SDS[5] and work by Hormnirun et al.[36] Merta and Stenius showed that as far as purely ionic effects go for cationic polymers adding SDS is equivalent to adding a simple electrolyte.[37] Because PVP is neutral and unaffected by ionic strength, the change in scattering must be due to an association of PVP with SDS below the CAC.

The behavior of η_r is very roughly a mirror image of the light-scattering behavior, except that the maximum occurs at a higher c_{SDS} than it does for light scattering and the subsequent decrease in η_r is less than the corresponding increase in the scattering. The increasing η_r is consistent with the idea of a swelling coil and of increased hydrodynamic volume as the PVP becomes increasingly charged by the SDS. Although the effect here is not as pronounced as it is in the scattering intensity, η_r begins to increase immediately upon addition of SDS (i.e., below the CAC). The location of the critical points in the η_r and light-scattering data do not have obvious interpretations, although the natural tendency is to assign them to the CMC (or CAC) and to the saturation point of SDS.

In fact, Hormnirun et al.[36] and Godard[6] found a similar maximum in the specific viscosity η_{sp} (in this case, $\eta_{sp} \propto \eta_r$ because $\eta_r = \eta_{sp}/c_p$ (Figure 2a)) for a system of hydroxypropylcellulose (HPC) and hexadecyltrimethylammonium bromide (HTAB) using discrete samples and Cannon−Ubbelohde viscometers. The concentration of HTAB at which the maximum occurred was proportional to c_{HPC} and independent of NaCl concentration. The authors attributed the maximum to the PSP of HTAB with HPC and the subsequent viscosity decline with increasing c_{HTAB} to electrostatic shielding of the saturated PSA as additional surfactant increased the ionic strength. This ionic-strength argument is the same as that used by Minatti et al.[15] to describe the decline in A_2 in the SDS/PEO system. Merta and Stenius also found similar maxima in η_r for cationic starch and ionic surfactants[37] and mixed ionic surfactants[38] under certain conditions, followed by a phase change to a gel.

Figure 2b shows scattering intensity versus c_{SDS} for different concentrations of 1 MDa PVP with and without NaCl. The SDS scattering intensity is practically negligible compared to all the scattering data involving PVP. Scattering by the 0.004 g/cm^3 1 MDa PVP in water follows the trend for 0.002 g/cm^3 2 MDa PVP, except that it reaches a lower,shallower minimum and its absolute magnitude is lower at higher c_{SDS}. This behavior can be ascribed to the A_3 term in eq 11, which increases as a function of c_p^2 and lowers the scattering intensity.

The shapes of the scattering-intensity curves for 0.0002 g/cm^3 1 MDa PVP in pure water and 0.002 g/cm^3 1 MDa PVP in 20 mM NaCl (Figure 2b) bear an interesting resemblance to each other but are markedly different from the 0.002 and 0.004 g/cm^3 data in pure water. The higher scattering intensity in 20 mM NaCl is due to the salt decreasing the values of A_2 and A_3. The fact that scattering intensity begins to decrease after a certain value of c_{SDS} is qualitatively consistent with the cross-term behavior in eq 6. The cross-term, which decreases the scattered

(36) Hormnirun, P.; Sirivat, A.; Jamieson, A. M. *Polymer* **2000**, *41*, 2127.

(37) Merta, J.; Stenius, P. *Colloids Surf., A* **1997**, *122*, 243.

(38) Merta, J.; Stenius, P. *Colloids Surf., A* **1999**, *149*, 367.

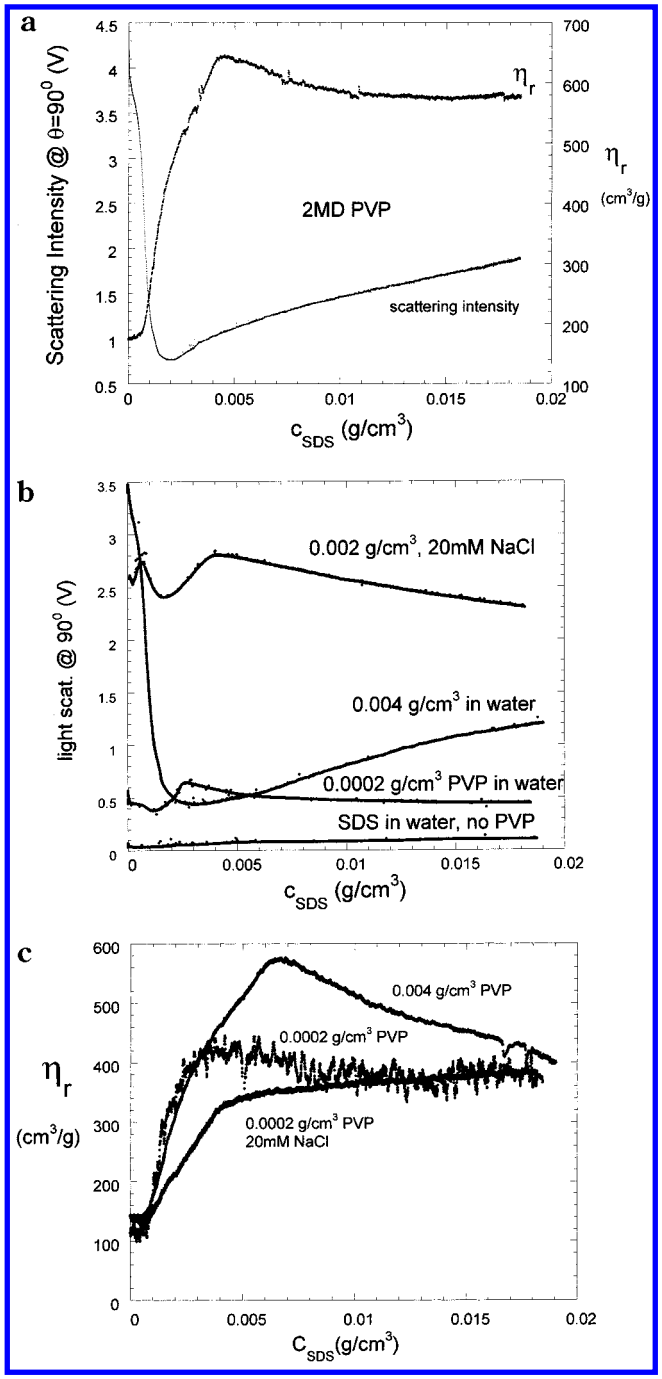

Figure 2. (a) Raw light-scattering and viscosity data for 2 MDa PVP vs c_{SDS} with no added salt. ($\eta_r = \eta_{sp}/(c_{PVP} = 0.002$ g/cm^3). (b) Raw light scattering vs c_{SDS} for 1 MDa PVP under a variety of solvent and concentration conditions. Also shown is the very weak scattering from pure SDS. (c) Viscosity data vs c_{SDS} for 1 MDa PVP under a variety of solvent and concentration conditions.

intensity, can become significant both for low $A_{2,a,a}$ values (caused by increased salt concentration) and for low PSA concentrations.

Figure 2c shows η_r versus c_{SDS} for the same solutions as in Figure 2b. Because $\eta_r = \eta_{sp}/c_p$, all the data are represented on the same graph. The qualitative effect of adding SDS is that viscosity increases; however, this increase is not as great when NaCl is present. This result is consistent with the notion that SDS binding to PVP increases the hydrodynamic volume, but the increase is measurably less when salt is present to shield the associated micelles on the SDS. η_r reaches a higher

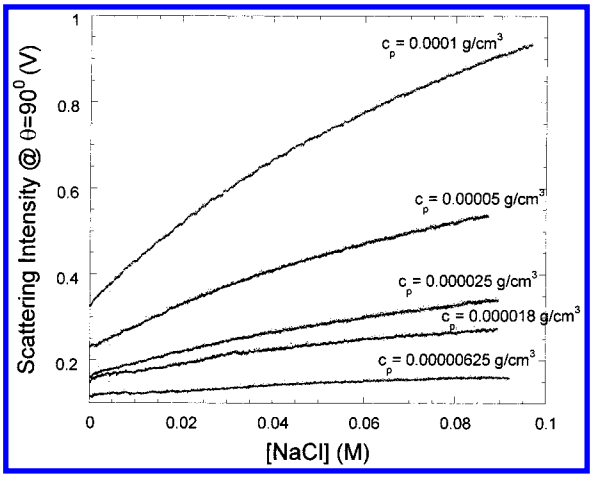

Figure 3. Raw light-scattering data vs [NaCl] for 1 MDa PVP at different concentrations, under saturating SDS conditions. $c_{SDS} = 0.01$ g/cm^3.

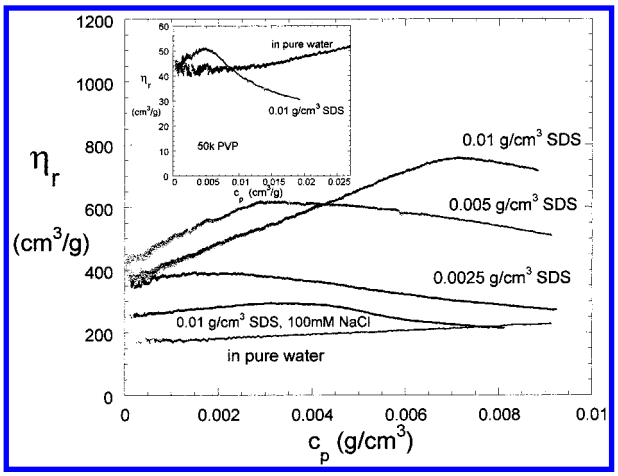

Figure 4. η_r vs c_p for 1 MDa PVP in a variety of solvents. Inset shows data for 50 kDa PVP with and without SDS.

maximum value for 0.004 g/cm^3 PVP because there is more PVP available for association before saturation. The decrease in η_r after the maximum value in pure water is attained can be attributed to increasing ionic strength after saturation.

Figure 3 shows raw light-scattering data for 360 kDa PVP at varying concentrations versus NaCl concentration. The increase shows the combination of two effects: an increase in PSA mass and a decrease in A_2. These effects will be separated below by individually extrapolating the Kc/I intercept to $q = 0$ and $c_p = 0$ for each value of the NaCl concentration.

Data Interpretation and Modeling. The raw data provide considerable grist for analysis. It is beyond the scope of this work to explore all possible models and relationships; therefore, our attention is confined to the most salient features concerning electrostatic and viscosity effects.

Figure 4 shows η_r versus c_p for the data of Figure 1b, where the inset is for 50 kDa PVP. The major features are that for the 1 MDa PVP both η_r and the intercept (η_r extrapolated to $c_p = 0$) are significantly higher and the value of η_r is maximized when SDS is present. For the 50 kDa PVP (inset to Figure 1b), the intercept (η_r extrapolated to $c_p = 0$) is the same (within error) whether SDS is present or not, and η_r in SDS drops below the corresponding value in pure water.

Extrapolation at low c_p allows computation of κ_{H1} without explicit knowledge of r:

$$\kappa_{H1} = \frac{\left(\frac{d\eta_r}{dc_p}\right)}{(\eta_r(c_p = 0))^2} \qquad (32)$$

The values of the intercept and slope for η_r are given in Table 2. Figure 5 shows R_g^3 versus c_p for the data from Figure 4, as computed via eq 30, using the values of κ_{H1} in Table 2. In pure water, R_g^3 is constant, as expected for a neutral polymers in the dilute and semidilute regimes. In all the other cases, R_g^3 is constant until a certain value of c_p is reached, after which point R_g^3 declines. This behavior suggests that the PVP is saturated with SDS and that the mass and hydrodynamic volume of the PSA are unaffected by increasing c_p until the point where the decline begins. After this point, desaturation of the PSA increases with increasing c_p, leading to a decrease in V_H as electrical charging of the PSA decreases.

The value of R_g on the plateau is also shown in Figure 5. It is less than the R_g from light scattering. The difference may be due to polydispersity, because light scattering measures $\langle S^2 \rangle_z$, and to the fact that the Flory−Fox equation applies to solutions at the Θ point.

The "break points" in Figure 5, seen as inflection points in Figure 4, at which both η_r and R_g^3 begin to decrease are useful measures of saturation of PVP by SDS. In the case of no added salt, $c_{SDS}/c_r = 1.1$, 1.78, and 1.45 for 0.0025, 0.005, and 0.01 g/cm^3 SDS, respectively, while for added salt and 0.01 g/cm^3 SDS, $c_{SDS}/c_r = 3.12$.

The maximum in η_r versus c_p in Figure 4 is reminiscent of the electroviscous effect that occurs in polyelectrolyte solutions when they are diluted with a solvent of fixed, very low ionic strength.[39−41] Although the effect seen here with the PSA is similar to the electroviscous effect, it seems that the origin must be significantly different because the qualitative conditions for its appearance are different. First, the maximum exists for PSA even at high ionic strength (see the data for 100 mM NaCl in Figure 1b), whereas for linear polyelectrolytes, it normally vanishes even at ionic strengths as low as 1 mM.[42] Second, the maximum appears at values of c_p on the order of 0.001−0.01 g/cm^3, whereas in linear polyelectrolyte solutions, the maximum appears at least an order of magnitude lower in c_p.

Figure 6 shows the electroviscous effect for xanthan obtained by the automatic dilution technique using pure water. The maximum occurs at about 4×10^{-5} g/cm^3, 2 orders of magnitude lower than that for the PSA in Figure 4. Also, this effect in xanthan is destroyed by polyelectrolytes of low ionic strength.

The explanation usually invoked for the electroviscous effect in linear polyelectrolytes is that by diluting them with a constant ionic-strength solvent, the total solution ionic strength changes because the counterions of the polyelectrolyte contribute to the total solution ionic strength. Hence, when the polyelectrolyte and counterions are diluted, the ionic strength decreases, leading to swelling of the polyelectrolyte and increased interactions, and thus increased η_r (i.e., the total hydrodynamic volume of the polymer phase of the solution increases more quickly than the polyelectrolyte mass concentration decreases).[43] After sufficient dilution, there is no more change in the dimensions of the polyelectrolytes, so that η_r decreases

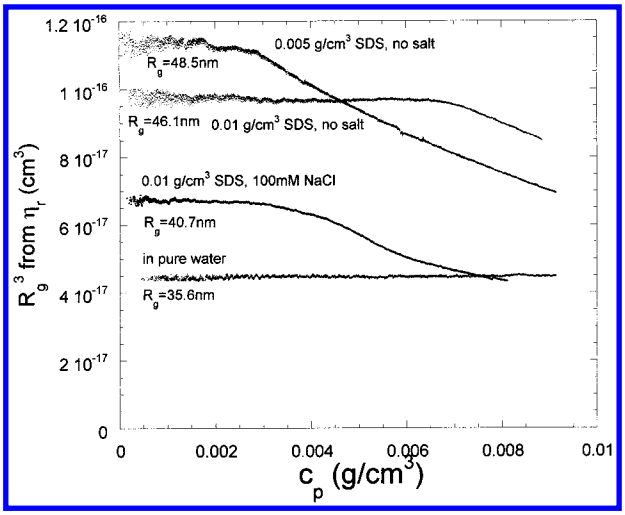

Figure 5. R_g^3 for 1 MDa PVP computed from η_r, according to eq 30, in a variety of solvents. Also shown is the plateau value of R_g (Å).

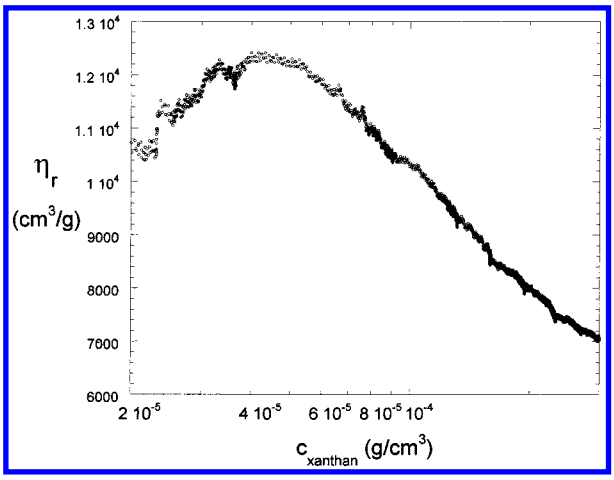

Figure 6. Electroviscous effect for xanthan measured with the automatic dilution technique. The concentration and ionic strength at which it occurs are entirely different from those involving PSA.

with further dilution as it does for neutral polymers. In the case of PSA, the decrease in c_p at a fixed SDS concentration has quite a different effect. Namely, decreasing c_p leads to more SDS per polymer, effectively increasing the net charge and hence the net R_g and V_H. η_r increases as c_p decreases because the increase of V_H occurs more quickly than the decrease of $[\eta]$ due to the increasing mass of the PSA as more SDS become associated. At low enough c_p, the PVP is saturated; therefore, R_g and V_H are stable and η_r decreases as it does for a neutral polymer. The similarity between the PSA and linear polyelectrolyte cases is that dilution leads to an increase in hydrodynamic volume, and the hydrodynamic volume increases more quickly than the mass concentration decreases. The difference is that in the case of the linear polyelectrolyte the increase in V_H with decreasing ionic strength is due to the increase in the solution ionic strength, whereas in the PSA case, the increase in V_H is due to the expansion of R_g caused both by the charging of the PVP as a result of increased SDS concentration and by the accretion of more volume by the SDS itself.

Presumably, it is this difference in mechanism controlling V_H that allows the electroviscous effect to occur in PSA under concentration and ionic-strength conditions that are radically different than those of linear polyelectrolytes. It is also important to note, as in ref 15, that the

(39) Basu, S. *Nature* **1951**, *168*, 341.
(40) Fuoss, R. M.; Strauss, V. P. *J. Polym. Sci.* **1948**, *3*, 602.
(41) Förster, S.; Schmidt, M. *Adv. Polym. Sci.* **1995**, *120*, 51.
(42) Rinaudo, M.; Milas, M.; Jouon, M.; Borsali, R. *Polymer* **1993**, *34*, 3710.
(43) Reed, W. F. *J. Chem. Phys.* **1994**, *101*, 2515.

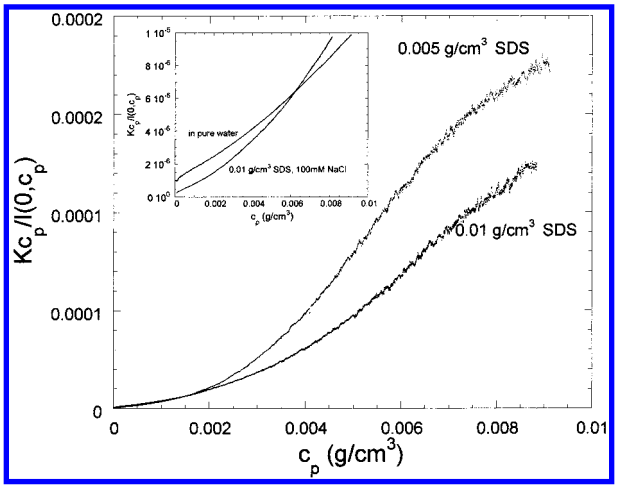

Figure 7. $Kc_p/I(0,c_p)$. $q = 0$ extrapolations of $Kc_p/I(q,0)$ for 1 MDa PVP are carried out in a variety of solvents. The contrast in magnitude with no added salt is so great that the cases with salt and without SDS are shown in the insets, for clarity.

light-scattering angular envelope of the PSA in salt-free solutions shows no maximum or negative slope as is normally found for many polyelectrolytes.[44−47] The origin of the light-scattering maxima has been ascribed to various mechanisms, including highly damped, quasi-periodic interparticle potentials in very low ionic strength solutions.[48] Although there have been attempts in the past to link the electroviscous effect to the maximum in light scattering, others have shown that the phenomena can exist independently of each other. The current case of the PSA is another illustration where an electroviscous effect can exist without the corresponding existence of a light-scattering maximum.

Figure 7 shows $Kc_p/I(0,c_p)$ for the data of Figure 1a. These data were obtained by extrapolating $Kc_p/I(q,c_p)$ versus q^2 to $q = 0$ at each value of c_p. The magnitude of $Kc_p/I(0,c_p)$ is so much greater when SDS is present with no added salt that the cases of PVP in pure water and with 0.01 g/cm^3 SDS in 0.1 M NaCl are shown in the inset, for clarity. The quadratic form of $Kc_p/I(0,c_p)$ is pronounced in all the curves, which is direct evidence of the effect of A_3 and gives a c_p^2 dependence (eq 10). For the cases of SDS where no salt is present, there is an inflection point in each curve, and the quadratic dependence is lost. The fact that the curves are well described by a second-order polynomial fit until close to the inflection point implies that M_w, A_2, and A_3 are essentially constant over the c_p range. The data show a negative second derivative as A_2 and A_3 decrease because of the desaturation of the PSA.

A_2, A_3, and $1/M_w$ before the inflection point can all be determined from data in Figure 7. The values of A_2, A_3, r, and ϵ are computed as follows and are shown in Table 2. First, r is computed by finding the value of $Kc_p/I(0,0)$ and using eq 19 in this limit with the value of $M_{w,p}$ from Table 1. The value of A_2 is then determined using the value of r and a linear fit to $Kc_p/I(0,c_p)$ over the linear regime found at low c_p. A_3 is determined in two ways: First, it can be obtained from r and the second-order coefficient of $Kc_p/I(q,c_p)$ via eq 21. Second, it can be determined directly by finding the concentration where $I(q = 0,c)$ has a maximum value, according to eq 31. $I(q = 0,c)$ is determined from the extrapolation of $Kc/I(q,c)$ to $q = 0$, taking the reciprocal of this function and multiplying by Kc. The peak of $I(q = 0,c)$ resembles that in Figure 2a (at $\theta = 90°$), except that the maximum occurs at a lower concentration. Whereas A_2 resulting from association and electrostatic effects without salt is enhanced by about a factor of 5 compared to pure 1 MDa PVP, A_3 increases by more than a factor of 30.

The difference in the A_3 values may in part be due to small A_4 effects. Corrections for A_4 were ignored here, however, because there was a negligible difference in quality between second- and third-order polynomial fits to $Kc_p/I(0,c_p)$.

A_3 for a sphere is related to A_2 via[49]

$$A_3 = \epsilon \frac{5MA_2^2}{8} \tag{33}$$

where $\epsilon = 1$ for a sphere. For coil polymers, this equation usually overestimates A_3 by 1.8−5, so that $\epsilon < 1$. ϵ is determined by comparing the experimental A_3 with A_2; values are listed in Table 2 for A_3 determined as previously described. The values of ϵ are ˜0.2−0.4, which are consistent with many experimental reports but are closer to the Stockmayer−Casassa[50] asymptotic value of about 0.65 than to the Yamakawa limit of 1.333.[51] These latter theories predict ϵ to be a monotonically increasing function, starting at zero, of the excluded-volume parameter z.[51]

With these values of ϵ and a model for r derived from the data, it is possible to estimate A_2 along the different curves in component coordinates by solving the resulting quadratic equation in A_2:

$$\frac{Kc_p}{I_{PSA}(0, c_p)} = \frac{1}{(1 + \delta r)^2}\left\{\frac{1}{M_{w,p}} + 2A_2c_p(1 + r)^2 + \frac{15\epsilon M_{w,p}A_2^2}{8}c_p^2(1 + r)^3\right\} \tag{34}$$

Figure 8 shows an example of this computation for A_2 versus c_{SDS} for the case of 0.004 g/cm^3 1 MDa PVP with no added salt. In the computation, ϵ was assumed to be constant, and r was taken as increasing linearly up to the PSP, after which it remained constant. This treatment gives a more quantitative basis to the claims made concerning the trends in the raw data. A_2 increases rapidly as SDS binds to PVP, even below the CAC, then declines after saturation; added SDS serves primarily to increase the solution ionic strength.

The inset to Figure 8 provides a quantitative illustration of the effects that electrostatic interactions have on excluded volume and on hydrodynamic interactions. R_{eq}' was computed from A_2 in Figure 8 via eq 36, and $R_{g,\eta}$ is the viscosity-based equivalent radius of gyration computed from the data in Figure 2c via eq 30. Both radii increase as c_{SDS} increases until a maximum value is reached, presumably near the PSP. After this point, each radius declines with increasing c_{SDS}. Also shown is $R_{eq}'/R_{g,\eta}$, which increases from about 1.15 to 1.6 then slowly decreases to 1.3. In other words, electrostatically charging the PSA by increasing c_{SDS} has a significantly larger effect on the

(44) Nierlich, M.; Williams, C. E.; Boue, F.; Cotton, J. P.; Daoud, M.; Farnoux, B.; Jannink, G.; Picot, C.; Moan, M.; Wolff, C.; Rinaudo, M.; de Gennes, P. G. *J. Phys. (Paris)* **1979**, *40*, 701.
(45) Drifford, M.; Dalbiez, J. P. *J. Phys. Chem.* **1984**, *88*, 5368.
(46) Li, X.; Reed, W. F. *J. Chem. Phys.* **1991**, *94*, 4568.
(47) Morfin, I.; Reed, W. F.; Rinaudo, M.; Borsali, R. *J. Phys. II* **1994**, *4*, 69.
(48) Norwood, D. P.; Benmouna, M.; Reed, W. F. *Macromolecules* **1996**, *29*, 4293.
(49) Hansen, J. P.; McDonald, I. R. *Theory of Simple Liquids*; Academic Press: New York, 1986.
(50) Stockmayer, W. H.; Casassa, E. F. *J. Chem. Phys.* **1952**, *20*, 1560.
(51) Yamakawa, H. *Modern Theory of Polymer Solutions*; Harper & Row: New York, 1971.

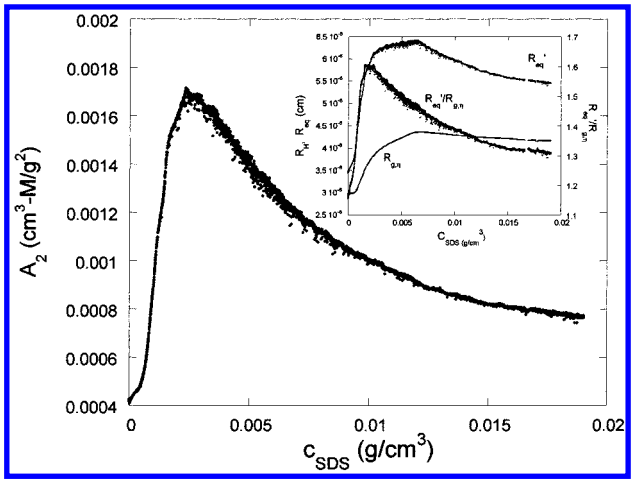

Figure 8. Estimated values of A_2 vs c_{SDS}, according to eq 34, for 1 MDa PVP at 0.004 g/cm^3 without salt (data from Figure 2a). The inset shows the equivalent radius of interparticle exclusion R_{eq}' and the hydrodynamic radius $R_{r,\eta}$. Also shown is $R_{eq}'/R_{r,\eta}$, for which it is seen that the electrostatic effect is significantly greater on the interparticle excluded volume than on the single-particle hydrodynamic radius.

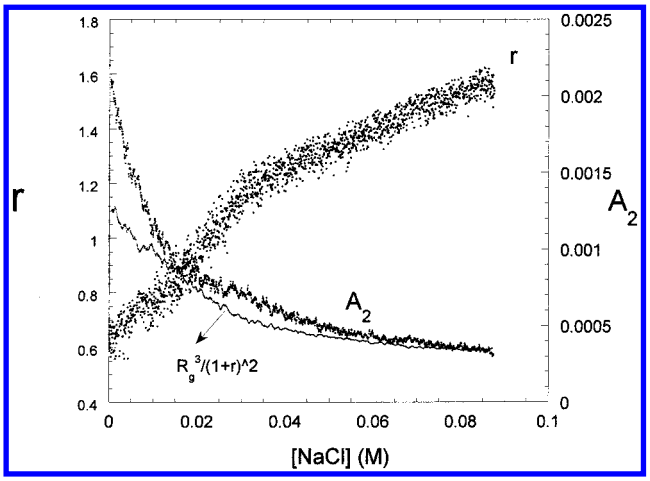

Figure 9. r and A_2 as a function of [NaCl] for 1 MDa PVP, obtained from extrapolations to $c_p = 0$ of data from Figure 3. Also shown is the quantity $R_g^3/(1 + r)^2$, as explained in the text. The deviation between $R_g^3/(1 + r)^2$ and A_2 is a measure of the component of A_2 due to the electrostatic field between PSA molecules.

interparticle excluded volume than on the hydrodynamically equivalent radius of individual particles and their hydrodynamic interactions.

The raw data of Figure 3 allows determination of r versus [NaCl] to be made via eq 19; subsequently, A_2 may be determined via eq 21. The data were measured under conditions in which the PVP was saturated by SDS. The concentrations of PVP used were too low, however, to obtain reliable viscosity data. Figure 9 shows both r and A_2 versus [NaCl]. r increases by nearly a factor of 3 in going from no added salt to moderate ionic strength. This result is qualitatively reasonable because the more highly charged micelles are expected to associate more strongly with the PVP the more they are shielded from each other. The initial value of A_2 is about six times higher than its pure PVP value. At moderate ionic strength, $A_2 \approx A_2$ in pure PVP. In Figure 9, A_2 decreases with increasing [NaCl], and in Figure 8, the decrease in A_2 after the maximum also follows the same decay behavior as in c_{SDS}. These findings are further evidence that the effect of SDS on the electrostatically enhanced properties of the PSA

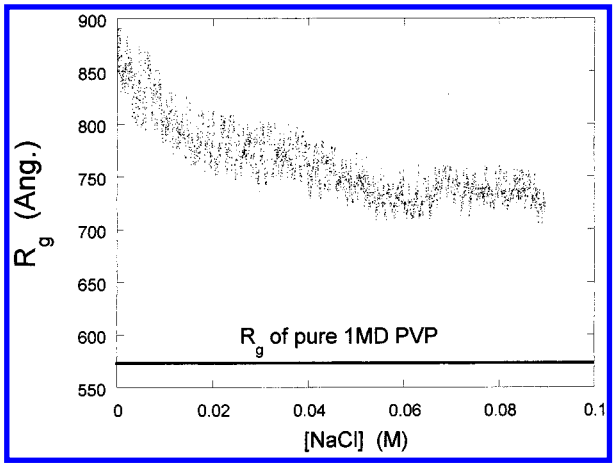

Figure 10. R_g vs [NaCl] from the data of Figure 3 for 1 MDa PVP at saturating SDS conditions (c_{SDS} = 0.01 g/cm^3). Also shown is the value of R_g for pure PVP.

after the PSP is equivalent to the effect of added salt. An approximate power law has been found for linear polyelectrolytes[52,53] and serves as a limit in combining electrostatic excluded-volume and persistence-length theories.

Figure 10 shows R_g versus [NaCl] for 1 MDa PVP, with a saturating level of SDS (c_{SDS} = 0.01 g/cm^3). R_g decreases modestly as [NaCl] increases, but it is always larger than R_g for pure PVP (570 Å), whose constant value is also shown in the Figure. This behavior suggests that a significant portion of the PSA swelling is purely due to steric factors. A modest decrease in both R_{eq}' and $R_{g,\eta}$ was also seen in the inset to Figure 8. Also shown on Figure 9 is the quantity $R_g^3/(1 + r)^2$, which was matched to the A_2 value at the highest ionic strength. In principle, this quantity should be proportional to A_2 if the excluded volume is controlled completely by R_g. While this quantity follows the trend in A_2, A_2 is consistently higher, which suggests that the electrostatic or "soft" part of the excluded volume is measurably greater than the "hard" part due to R_g. A_2 consists of the hard excluded volume due to an equivalent sphere of radius R_{eq}', whereas the soft part of A_2 is contained in $\int_{2R_{eq}'}^{\infty}[1 - \exp(-U_{el}(r_{12})/k_BT]]r_{12}^2 dr_{12}$.

$$A_2 = \frac{N_A}{2M^2}\left[\frac{32\pi R_{eq}^{\ 3}}{3} + 4\pi\int_{2R_{eq}}^{\infty}[1 - \exp(-U_{el}(r_{12})/k_BT]]r_{12}^2 dr_{12}\right] \quad (35)$$

r_{12} is the distance between the center of the equivalent spheres and $U_{el}(r_{12})$ is the interparticle electrostatic potential energy. While measurable, the enhancement of A_2 due purely to the electrostatic integral term is relatively modest for the PSA. In the case of pure CTABr micelles, purely electrostatic enhancement of nearly 2 orders of magnitude was found for A_2 in going from high to low ionic strength.[54]

Referring to Figure 4, it is interesting that η_r versus [PVP] is essentially linear, showing that intrinsic viscosity and two-body interactions are dominant hydrodynamically, whereas the pronounced upward curvature of Kc/I shows that three-body interactions become dominant in

(52) Reed, W. F.; Ghosh, S.; Medjahdi, G.; François, *Macromolecules* **1991**, *24*, 6189.
(53) Ghosh, S.; Li, X.; Reed, C. E.; Reed, W. F. *Biopolymers* **1990**, *30*, 1101.
(54) Baptista, M. S.; Politi, M. J.; Cuccovia, I.; Chaimovich, H. G.; Reed, W. F. *J. Phys. Chem.* **1992**, *96*, 6442.

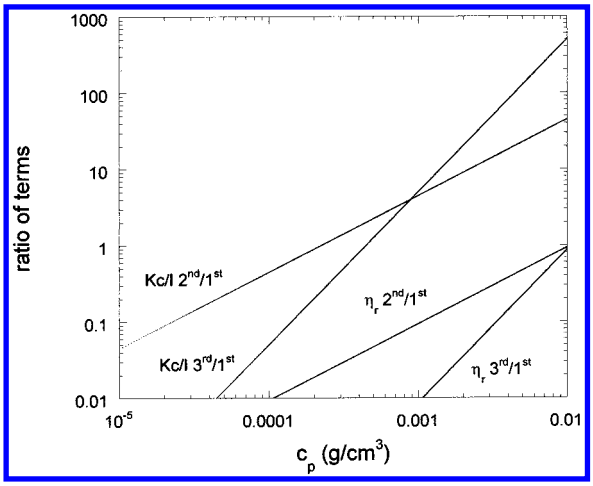

Figure 11. Comparison of second- and third-order terms for both light scattering and viscosity. Parameter values are given in the text. Strikingly, third-order light-scattering terms grow to nearly 3 orders of magnitude greater than the first-order term, whereas the third-order viscosity terms are comparable to the first-order term.

terms of interparticle excluded volume. This result is consistent with the previous notion that the electrostatic field contributes a significant soft component to A_2 and A_3, whereas the interparticle electrostatic field probably does little to affect fluid flow around the polymers.

A_2 for a polymer coil can be represented via the excluded-volume interactions of an equivalent sphere of radius R_{eq}' (which includes both terms on the right side of eq 35):

$$A_2 = \frac{16\pi N_A (R_{eq}')^3}{3M^2} \tag{36}$$

R_{eq}' is usually significantly smaller than R_g.[51] The ratio of the magnitude of two-body to single-body terms in Kc/I is

$$W_{2:1,LS} \equiv 2A_2 c_p M \tag{37}$$

whereas for the viscosity

$$W_{2:1,\eta_r} \equiv \kappa_{H1}[\eta]c_p \tag{38}$$

Figure 11 shows the dramatic difference between the ratios of second- to first-order terms for Kc/I and η_r using parameters typical for the PSA: $A_2 = 10^{-3}$, $M = 10^6$, $r = 0.5$, $[\eta]_{PSA} = 250$, and $\kappa_{H1} = 0.25$

Using the previous expressions for A_2 and η_r gives

$$\frac{W_{2:1,\eta_r}}{W_{2:1,LS}} = 0.187\kappa_H\left(\frac{R_{g,\eta_r}}{R_{eq}'}\right)^3 \tag{39}$$

This ratio is about 10% for pure PVP or highly screened PVP, whereas for PSA with no added salt, the value is closer to 1%. Hence, the two-body effects in light scattering dominate even in neutral or highly screened systems but are an order of magnitude more dominant in lightly screened systems.

Using the equivalent hard-sphere expression for A_3 of eq 33 gives an expression for third- to second-order terms in Kc/I:

$$W_{3:2,LS} = \frac{3A_3 c_p}{2A_2} = \frac{15}{16} MA_2 c_p \approx \frac{W_{2:1,LS}}{2} \tag{40}$$

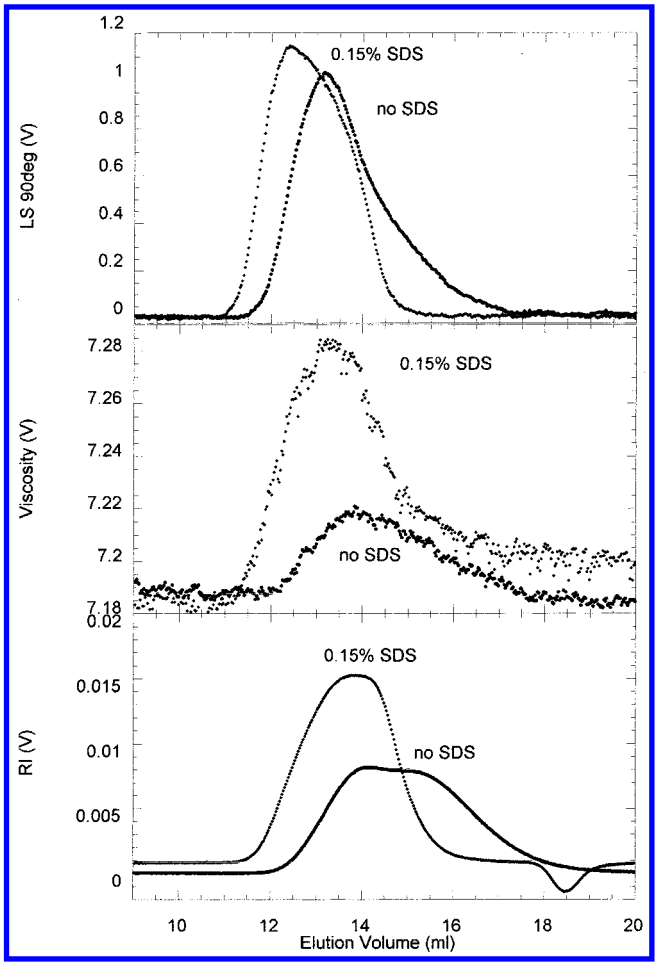

Figure 12. Raw GPC , light-scattering, viscometry, and refractometry data for 1 MDa PVP eluted in aqueous solvent with no SDS and in water with 0.0015 g/cm^3 SDS.

Hence $W_{3:2,LS}$ is on the order of $W_{2:1,LS}$; when the latter term significantly exceeds unity (as seen in Figure 11), the former term becomes dominant.

Unfortunately, no theoretical form of κ_{H2} exists for polymers, although empirical expressions exist.[55] For impenetrable hard spheres, $\kappa_{H2} = \kappa_{H1}^2$. Using this relationship as an approximation,

$$W_{3:2,\eta_r} \approx \kappa_{H1}[\eta]c_p \tag{41}$$

which has about the same value as $W_{2:1,\eta_r}$. Because this latter quantity is generally significantly less than unity (Figure 11), the third-order term has a virtually negligible effect on η_r.

Figure 11 also shows the magnitude of the third-order/first-order terms, whose values are based on the previously mentioned parameter values, on $A_3 = 0.5$, and on eq 41 with $\kappa_{H1} = 0.25$. the third-order light-scattering term is nearly 3 orders of magnitude larger than the first-order term (M_p) at $c_p = 0.01$ g/cm^3, whereas for viscosity, the second- and third-order terms are comparable to the first-order term.

Figure 12 shows raw GPC refractometry, light-scattering, and viscosity chromatograms for 1 MDa PVP in an eluent composed of pure water and aqueous 0.0015 g/cm^3 SDS. As expected when the SDS is present, the PVP refractive index chromatogram shifts to lower elution

(55) Bohdanecky, M.; Kovar, J. In *Viscosity of Polymer Solutions*; Jenkins, A. D., Ed.; Polymer Science Library 2, Elsevier Science: New York, 1982.

volumes, which is consistent with higher hydrodynamic volume and mass. Scattering intensity increases measurably, although there is still significant A_2 suppression of light scattering even at the low concentrations involved, and the viscosity signal is markedly higher when SDS is present than for PVP in pure water. All these trends are consistent with those found by the automatic dilution technique. It was implicitly assumed throughout this work that SDS interacts equally with all polymers and that no bimodal distribution of PSA and bare PVP occurs. This supposition is confirmed by the chromatograms, which show that all the PVP moves to lower elution volumes.

Conclusions

The ensemble of effects leads to the following conclusions. The formation of PSA is apparent from both continuous viscosity and light scattering monitoring. The PSA begin to form immediately as SDS is added to a solution of PVP and begin to turn the PVP into a pseudopolyelectrolyte, even before the CAC. The changes in the mass, intrinsic viscosity, and A_2 are moderate, on the order of up to a few hundred percent. Very distinct signatures in the presence of SDS, however, set the data apart from those due to PVP alone. The most distinct features are (1) decreasing scattered light with increasing c_{SDS} at fixed c_p because of the electrical charging and increasing A_2 and A_3 of the PSA, (2) well-defined maxima in scattering versus c_p curves under saturating SDS conditions because of the electrostatic enhancement of A_3, and (3) maxima in the reduced viscosity versus c_p curves when the PSA become saturated with SDS. This latter effect bears a certain resemblance to the electroviscous effect observed for linear polyelectrolytes, although the mechanism and regimes of occurrence are very different. The saturation ratio of SDS/PVP increases as ionic strength increases, which shows that increased screening allows for more association of the anionic SDS with the neutral PVP. The PSA have R_g values up to about twice the R_g values of pure PVP, but R_g is relatively insensitive to ionic strength compared to the stronger ionic-strength dependences of r and A_2. The data provide an interesting example of how three-body effects in light-scattering A_3 can be orders of magnitude larger than three-body effects in viscosity. In all instances, the effect of electrostatics on the interparticle excluded volume is significantly greater than its effect on the hydrodynamic radius.

It is hoped that the automatic dilution technique will prove useful for a wide variety of studies involving polymer and surfactant interactions.

Acknowledgment. Support from the U.S. National Science Foundation (Grant CTS 9877206) is acknowledged.

LA0109718